Reconstructing Past Seawater Mg/Ca and Sr/Ca from Mid-Ocean Ridge Flank Calcium Carbonate Veins

Rosalind M. Coggon, *et al.*

Science **327**, 1114 (2010);
DOI: 10.1126/science.1182252

Science (print ISSN 0036-8075; online ISSN 1095-9203) is published weekly, except the last week in December, by the American Association for the Advancement of Science, 1200 New York Avenue NW, Washington, DC 20005.

the amount of catalyst in the oligomerization reactor modifies the selectivity, decreasing the C_8-C_{16} fraction and increasing the percentage of larger alkenes [see table S2 and related text (*23*)].

The integrated system reported here for conversion of GVL to liquid alkenes in the transportation fuel range consists of two flow reactors, two phase separators, and a simple pumping system for delivery of an aqueous solution of GVL, thereby minimizing secondary processing steps and equipment (e.g., purification of feeds, compression and pumping of gases). In addition, this approach does not require the use of precious metal catalysts, further decreasing capital costs. The catalytic system described in this report provides an efficient and inexpensive processing strategy for GVL. The cost of producing either butene or jet fuel with the approaches described here would be governed by the market value of GVL, and further research should be carried out toward optimizing production of GVL from renewable biomass resources, thereby minimizing the cost of the GVL feed to our process, and toward utilization of the high-pressure CO_2 coproduct stream formed in our process. Additionally, the yield of high molecular weight alkenes from GVL would benefit from the development of water-tolerant oligomerization catalysts.

References and Notes

1. E. L. Kunkes *et al.*, *Science* **322**, 417 (2008).
2. A. J. Ragauskas *et al.*, *Science* **311**, 484 (2006).
3. G. W. Huber, S. Iborra, A. Corma, *Chem. Rev.* **106**, 4044 (2006).
4. D. A. Simonetti, J. Rass-Hansen, E. L. Kunkes, R. R. Soares, J. A. Dumesic, *Green Chem.* **9**, 1073 (2007).
5. G. W. Huber, B. E. Dale, *Sci. Am.* **301**, 52 (2009).
6. I. T.Horváth, H. Mehdi, V. Fábos, L. Boda, L. T. Mika, *Green Chem.* **10**, 238 (2008).
7. H. Mehdi *et al.*, *Top. Catal.* **48**, 49 (2008).
8. L. E. Manzer, *Appl. Catal. Gen.* **272**, 249 (2004).
9. S. W. Fitzpatrick, "Final Technical Report: Commercialization of the Biofine Technology for Levulinic Acid Production from Paper Sludge," *Tech. Report No. DOE/CE/41178* (BioMetics, Inc, Waltham, MA, 2002); www.osti.gov/bridge.
10. H. Heeres *et al.*, *Green Chem.* **11**, 1247 (2009).
11. I. Ahmed, U.S. Patent 6,190,427 (2001).
12. D. C. Elliott, J. G. Frye, U.S. Patent 5,883,266 (1999)
13. G. W. Huber, "Breaking the Chemical and Engineering Barriers to Lignocellulosic Biofuels: Next Generation Hydrocarbon Biorefineries" (Univ. of Massachusetts Amherst, 2007); www.ecs.umass.edu/biofuels/Images/Roadmap2-08.pdf.
14. R. S. Haszeldine, *Science* **325**, 1647 (2009).
15. K. S. Lackner, *Science* **300**, 1677 (2003).
16. H. Sakurai, M. Haruta, *Catal. Today* **29**, 361 (1996).
17. J. Toyir, P. R. de la Piscina, J. L. G. Fierro, N. Homs, *Appl. Catal. Environ.* **34**, 255 (2001).
18. S. Koppatz *et al.*, *Fuel Process. Technol.* **90**, 914 (2009).
19. R. D. Cortright, R. R. Davda, J. A. Dumesic, *Nature* **418**, 964 (2002).
20. G. W. Coates, D. R. Moore, *Angew. Chem. Int. Ed.* **43**, 6618 (2004).
21. D. J. Darensbourg, *Chem. Rev.* **107**, 2388 (2007).
22. M. Wick, J. M. Lebeault, *Appl. Microbiol. Biotechnol.* **56**, 687 (2001).
23. Materials and methods are available as supporting material on *Science* Online.
24. S. Matar, L. F. Hatch, *Chemistry of Petrochemical Processes* (Gulf Professional Publishing, Houston, TX, ed. 2, 2000), pp. 248–250.
25. J. Čejka, H. van Bekkum, A. Corma, F. Schüth, in *Introduction to Zeolite Science and Practice* (Elsevier, Amsterdam, rev. ed. 3, 2007), pp. 895–899.
26. A. Mantilla *et al.*, *Catal. Today* **107-108**, 707 (2005).
27. R. J. Quann, L. A. Green, S. A. Tabak, F. J. Krambeck, *Ind. Eng. Chem. Res.* **27**, 565 (1988).
28. G. Centi, R. Van Santen, in *Catalysis for Renewables: From Feedstock to Energy Production* (Wiley-VCH, Weinheim, Germany, 2007), p. 137.
29. J. Skupinska, *Chem. Rev.* **91**, 613 (1991).

30. This work was supported through funding from the Defense Advanced Research Projects Agency (DARPA) (Surf-cat: Catalysts for Production of JP-8 range molecules from Lignocellulosic Biomass). The views, opinions, and/or findings contained here are those of the authors and should not be interpreted as representing the official views or policies, either expressed or implied, of DARPA or the Department of Defense. In addition, this work was supported in part by the U.S. Department of Energy (DOE), Office of Basic Energy Sciences, and by the DOE Great Lakes Bioenergy Research Center (www.greatlakesbioenergy.org), which is supported by the U.S. DOE, Office of Science, Office of Biological and Environmental Research, through Cooperative Agreement between The Board of Regents of the University of Wisconsin System and the U.S. DOE. A patent application has been filed in association with the Wisconsin Alumni Research Foundation based on the technology reported here. We thank R. Oakes, T. Reigle, and C. Skadahl for their assistance in our investigation of the production of butene from GVL.

Supporting Online Material

www.sciencemag.org/cgi/content/full/327/5969/1110/DC1
Materials and Methods
Figs. S1 to S4
Tables S1 and S2

6 November 2009; accepted 7 January 2010
10.1126/science.1184362

Reconstructing Past Seawater Mg/Ca and Sr/Ca from Mid-Ocean Ridge Flank Calcium Carbonate Veins

Rosalind M. Coggon,[1] Damon A. H. Teagle,[2]* Christopher E. Smith-Duque,[2] Jeffrey C. Alt,[3] Matthew J. Cooper[2]

Proxies for past seawater chemistry, such as Mg/Ca and Sr/Ca ratios, provide a record of the dynamic exchanges of elements between the solid Earth, the atmosphere, and the hydrosphere and the evolving influence of life. We estimated past oceanic Mg/Ca and Sr/Ca ratios from suites of 1.6- to 170-million-year-old calcium carbonate veins that had precipitated from seawater-derived fluids in ocean ridge flank basalts. Our data indicate that before the Neogene, oceanic Mg/Ca and Sr/Ca ratios were lower than in the modern ocean. Decreased ocean spreading since the Cretaceous and the resulting slow reduction in ocean crustal hydrothermal exchange throughout the early Tertiary may explain the recent rise in these ratios.

Cation ratios in seawater reflect the balance between their supply to and removal from the oceans, and these ratios can control important geochemical processes. For example, the influence of the seawater Mg/Ca ratio on calcium carbonate ($CaCO_3$) precipitation [high Mg/Ca ratios favor the formation of aragonite, whereas low Mg/Ca ratios favor calcite (*1*)] has important effects on marine biota and the distribution of carbonate sediments. Seawater chemistry has varied with global climate throughout Earth's history, making past seawater cation ratios such as Mg/Ca and Sr/Ca attractive proxies for determining paleo-ocean conditions (*2*–*4*). Previous estimates of seawater cation ratios have been developed from mass-balance modeling (*5*, *6*) and analyses of marine cements (*7*), fossils (*8*–*10*), and fluid inclusions trapped in halite (*11*–*13*). Unfortunately, marine sedimentary carbonates are susceptible to diagenesis (*14*), and reactions during halite formation may perturb elemental ratios from those of contemporaneous seawater, requiring careful sample selection and analysis (*11*).

Here we propose a new method for reconstructing past variations in seawater Mg/Ca and Sr/Ca ratios from the composition of $CaCO_3$ veins (CCVs) formed in oceanic crust, as recovered by ocean drilling (*15*). CCVs are formed as seawater flows through the upper ocean crust on mid-ocean ridge flanks and reacts with basalt (*16*). Calcite and aragonite precipitate from these fluids to form veins within the basement lavas (*17*). The cation composition of the carbonates therefore records the chemistry of the basement fluid, provided that the temperature at which the veins formed can be determined and the temperature dependence of element partitioning between fluid and mineral is known (*15*, *18*).

If CCVs form on ridge flanks with thin sediment cover at near-bottom water temperatures (<6°C), the reaction between seawater and basalt is minimal and the carbonate data define the seawater Mg/Ca and Sr/Ca ratios at the age determined by their $^{87}Sr/^{86}Sr$ ratios and the well-established seawater Sr isotope record (*19*). However, if CCVs form at moderate tem-

[1]Department of Earth Science and Engineering, Imperial College London, South Kensington Campus, Exhibition Road, London SW7 2AZ, UK. [2]School of Ocean and Earth Science, National Oceanography Centre, University of Southampton, Southampton SO14 3ZH, UK. [3]Department of Geological Sciences, University of Michigan, Ann Arbor, MI 48109-1005, USA.

*To whom correspondence should be addressed. E-mail: damon.teagle@soton.ac.uk

peratures (<60°C) on ridge flanks, where early, rapid sedimentation thermally blankets the basement (*20*), carbonates precipitate after substantial seawater-basalt exchange. The composition of the seawater is derived from the trends of evolving fluid chemistry versus temperature that are calculated for the suite of CCVs from a particular site by extrapolating back to the temperature of contemporaneous seawater (*15*). This was previously demonstrated for a suite of young CCVs from the 1.6- to 3.6-million-year-old Juan de Fuca Ridge (JdFR) basement, where a faithful record of the chemical evolution of near-basement pore waters during active ridge-flank circulation was preserved (Fig. 1) (*18*). In these samples, both the pore fluids and CCVs record fluid Sr/Ca, Mg/Ca, and $^{87}Sr/^{86}Sr$ ratios that show a progressive decrease from modern seawater values and indicate increased fluid-rock interaction with increasing temperature. These linear trends with temperature project back to the modern seawater values for each parameter.

We reconstructed past seawater Mg/Ca and Sr/Ca ratios from CCVs formed in 1.6- to 170-million-year-old upper ocean crust in the Atlantic and Pacific Oceans (table S1). CCVs from older crust, where the carbonate-precipitating hydrothermal systems are now extinct, mostly display similar behavior to that observed on the JdFR. For example, basement CCVs at site 843 precipitated at temperatures from 13° to 31°C from ~109-million-year-old fluids whose cation ratios and Sr isotope compositions varied with temperature (Fig. 1 and table S3). The preservation of chemical trends in ancient ocean crust gives confidence that basement CCVs are resistant to post-precipitation alteration. Consequently, the Sr/Ca, Mg/Ca, and $^{87}Sr/^{86}Sr$ ratios (and hence age) of the contemporaneous seawater from which the basement fluids developed are determined by the back extrapolation of the geochemical temperature trends recorded by the CCVs to the temperature of the contemporaneous bottom water (*15*) (Fig. 1).

From the reconstruction of seawater chemistry (Fig. 2), it is apparent that the Sr/Ca and Mg/Ca ratios were lower from the Middle Jurassic to the Oligocene than they are at present. We estimate that the molar Mg/Ca ratio of seawater remained around 1.5 to 2.5 between 170 and 24 million years ago (Ma) and then rose rapidly to ~5. Our independent record of past seawater Mg/Ca ratios from CCVs is generally in good agreement with seawater Mg/Ca records derived from evaporite inclusions (*11*–*13*) and echinoderm ossicles (*8*) (Fig. 2). We also observe that basalt-hosted CCVs that were precipitated during the Cretaceous and Paleogene are predominantly calcitic, whereas aragonite veins are more common in younger basalts with coexisting calcite veins that were generally precipitated at higher temperatures (>35°C) from fluids with lower Mg/Ca ratios produced by fluid rock exchange. This is in accordance with the greater abundance of aragonitic nonskeletal and biogenic marine carbonate since the early Cenozoic (*21*, *22*), which is attributed to an increase in the seawater Mg/Ca ratio (*22*). Similarly, the molar Sr/Ca ratio of seawater was relatively constant ($\sim 2.8 \times 10^{-3} \pm 1 \times 10^{-3}$) at approximately 30% of the modern value between 170 and 24 Ma before increasing to $\sim 8 \times 10^{-3}$ in the modern oceans. The correlations between estimated fluid Sr/Ca and temperature, and the similar estimates for ~80-million-year-old seawater Sr/Ca from sites in different oceans (for example, sites 1179 and 417/418) that had contrasting sedimentation histories, provide further support for this approach.

Our data suggest that the low Sr/Ca ratio of deep sea carbonates precipitated during the Cretaceous [~30% of modern carbonates (*23*)] is an original sedimentary signature (Fig. 2), resolving a long-standing debate. However, our seawater Sr/Ca determination is much lower than estimates based on benthic foraminifera and macrofossil calcite (*4*, *24*, *25*). We attribute this discrepancy to the great uncertainties in biogenic carbonate-Sr partitioning. Elemental partition coefficients are highly variable between different biominerals because of poorly understood physiological effects (*2*, *9*, *26*), and it is often necessary to assume that partition coefficients determined from modern biogenic carbonate are appropriate for past biomineralization and for species for which there are no modern equivalents. For example, Cretaceous and Jurassic seawater Sr/Ca ratios have been estimated from analyses of bivalves and belemnites using the average partition coefficient for modern brachiopods and bivalves (*10*). However, these coefficients vary by at least a factor of 4 (*24*, *27*) and are dependent on both temperature and calcification rate (*28*).

To evaluate the processes that are responsible for an increase in both the seawater Mg/Ca and Sr/Ca ratios since the Oligocene (Fig. 2), we consider the effects of changes in the magnitude and composition of the major ocean sources and sinks of these elements, namely river discharge, sediment burial, and hydrothermal exchange (Fig. 3). Past variation in the composition of global river discharge is difficult to quantify (*29*), but the discharge-weighted average composition of global rivers has most likely varied within the collective range of modern rivers (Fig. 3). The majority of modern rivers have

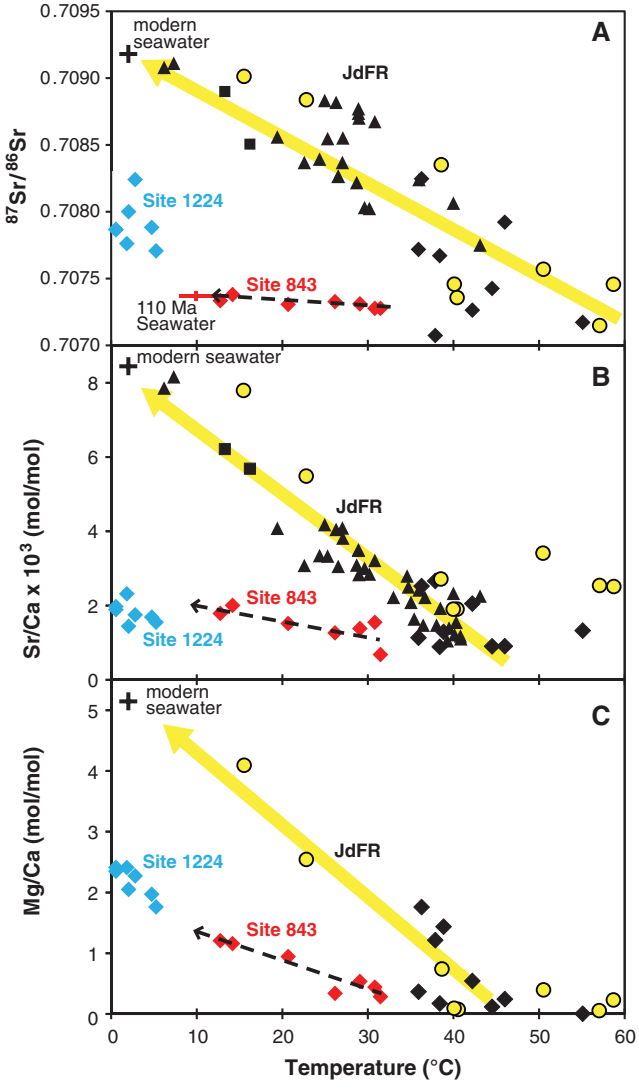

Fig. 1. Plots of fluid $^{87}Sr/^{86}Sr$ (**A**), Sr/Ca (**B**), and Mg/Ca (**C**) ratios against temperature for three sites showing contrasting styles of fluid evolution. Basement fluid compositions recorded by calcite (black diamonds), high-Mg calcite (black squares), and aragonite (black triangles) veins from the JdFR (*18*) record the same geochemical fluid evolution as near-basement pore fluids do [yellow circles (*16*)]. These trends extrapolate back to the composition of modern seawater (black cross), as indicated by the yellow arrows. CCVs from the warm 110-million-year-old site 843 crust (calcite; red diamonds) record fluid evolution trends that project back to ~10°C, 110-million-year-old seawater [red cross (*19*)] and have lower Sr/Ca and Mg/Ca ratios than modern seawater does. CCVs from the cool 46-million-year-old site 1224 crust [blue diamonds (*33*)] all precipitated at near-bottom seawater temperatures (<6°C) and are assumed to have undergone insignificant reaction with the basement.

Mg/Ca ratios that are lower than the Mg/Ca ratio of seawater since 170 Ma, whereas they display a much wider range of Sr/Ca ratios (Fig. 3). This suggests that a decrease in global river discharge in the Neogene would have increased the Mg/Ca ratio of seawater but not the Sr/Ca ratio. Decreased river discharge could therefore account for some of our proposed change in seawater composition.

The impact of sedimentation on seawater Sr/Ca and Mg/Ca ratios depends on mineralogy (Fig. 3A); conditions favoring the precipitation of calcite and aragonite have varied throughout the Phanerozoic (*21*). The most recent shift in the early Cenozoic, to conditions favoring aragonite precipitation, cannot account for our proposed increase in seawater Mg/Ca and Sr/Ca ratios (Fig. 3B). Post-burial alteration of carbonate may also affect the composition of seawater. Mg-Ca exchange during dolomite [$Ca,Mg(CO_3)_2$] formation would decrease seawater Mg/Ca, but its influence on seawater Sr/Ca depends on the carbonate mineral being altered and the time elapsed between deposition and dolomitization.

High-temperature black smoker–type reactions completely remove Mg from seawater during hydrothermal circulation and decrease the fluid Sr/Ca ratio (*30*), indicating that axial hydrothermal fluids should always have lower Sr/Ca and Mg/Ca ratios than contemporaneous seawater does. The major decrease (>30%) in ocean crust production rates (*31*) from the Cretaceous to the Tertiary and consequent lower black smoker fluid volumes would have increased seawater Sr/Ca and Mg/Ca ratios, albeit earlier than was observed in our record. Decreased low-temperature ridge flank hydrothermal alteration has a similar effect on seawater cation ratios. However, because of the vast area of the ridge flanks and the persistence of hydrothermal circulation for ~65 million years off axis, there

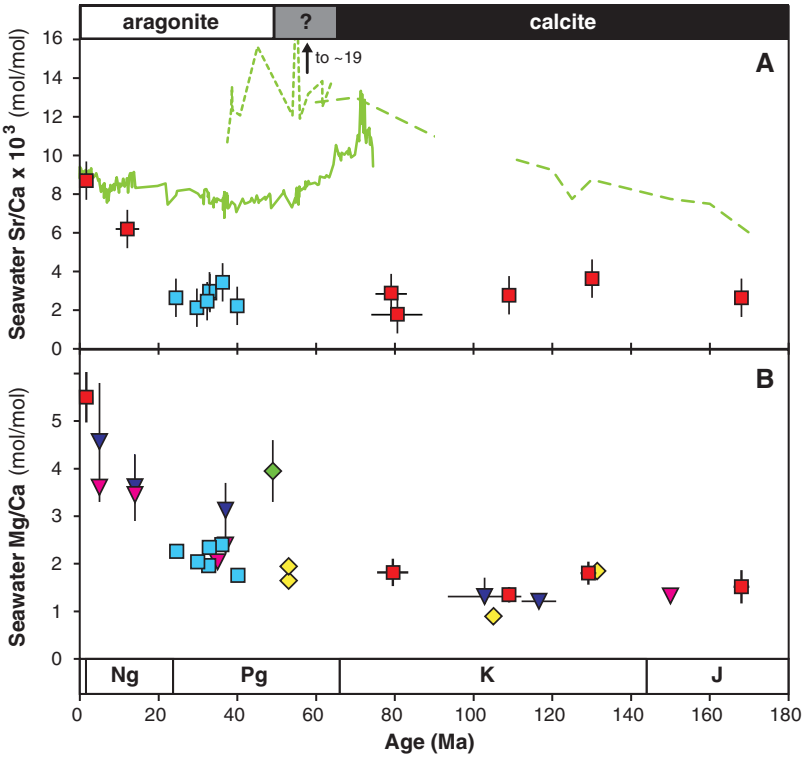

Fig. 2. Comparisons of past seawater cation ratios determined from CCVs from warm sites (red squares) and cool site 1224 (blue squares) with previous estimates of (**A**) seawater Sr/Ca estimates from benthic foraminifera [solid green line (*4*)], bivalves and belemnites [dashed green line (*10*)], and the minimum Sr/Ca estimated from marine turritellid snails [dotted green line (*25*)]; and (**B**) seawater Mg/Ca estimates from halite-trapped fluid inclusions [pink triangles (*11*) and dark blue triangles (*12*), Cretaceous estimates as updated by (*13*)], benthic foraminifera [green diamond (*9*)], and echinoderm ossicles [yellow diamonds (*8*)]. The upper bar indicates intervals when marine conditions favored the precipitation of calcite and aragonite (*21*), and the lower bar shows the geological periods. J, Jurassic; K, Cretaceous; Pg, Paleogene; and Ng, Neogene.

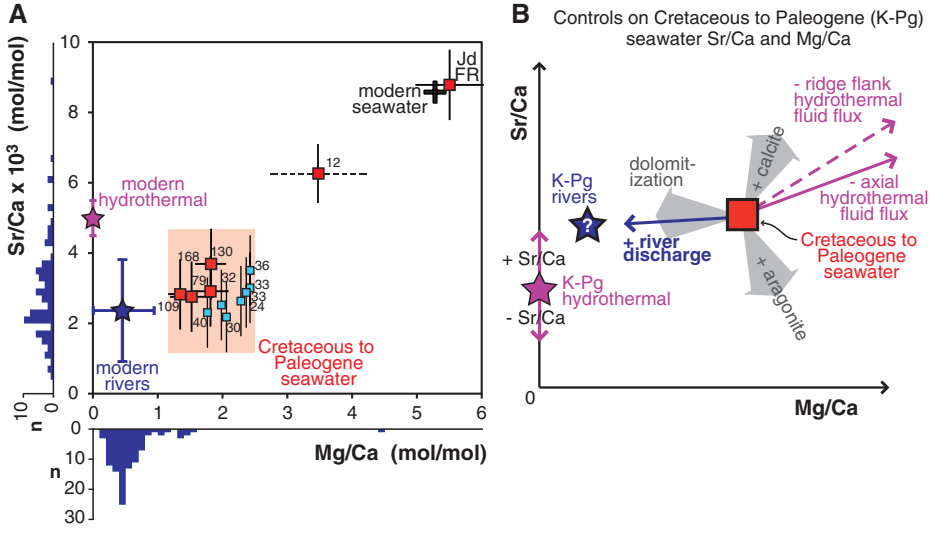

Fig. 3. (**A**) Variation in seawater Sr/Ca and Mg/Ca ratios with time recorded by CCVs [labels indicate age (Ma)] from warm ridge flanks (large red squares) and cool ridge flank site 1224 (smaller light blue squares) relative to modern seawater (black cross). Shown for comparison are the present-day ocean inputs from hydrothermal circulation [purple star; average black smoker fluid (*30*)] and rivers [dark blue star; discharge-weighted average river composition (*34*–*36*), ±1 SD]. The variability of modern river compositions is shown by the histograms along the figure's axes (*n* indicates number of rivers). The Mg/Ca ratio of 12-million-year-old seawater (dashed line) is estimated from evaporite fluid inclusion studies (*11*, *12*). The composition of seawater during the Cretaceous and Paleogene is highlighted (pink box). (**B**) Sketch illustrating the effects on the Sr/Ca and Mg/Ca ratios of Cretaceous-Paleogene (K-Pg) seawater of decreased axial or ridge flank hydrothermal fluid fluxes (purple arrows), or increased global river discharge (blue arrow), calcite or aragonite sedimentation, and dolomitization of sediments (gray arrows). We assume that K-Pg global river discharge (blue star) was compositionally similar to modern discharge. The effect of increasing (+) or decreasing (–) the Sr/Ca ratio of seawater on hydrothermal fluids (purple star) is illustrated.

will be a substantial delay in the impact of lower crustal production rates on decreased low-temperature fluid fluxes, because the age spectrum of the ridge flanks changes only slowly. Presently, only ~55% of the ocean floor is less than 65 million years old and contributes to ridge flank hydrothermal circulation, compared with ~85% in the Late Cretaceous (*32*). Decreasing fluid-rock exchange on the ridge flanks throughout the Tertiary, superimposed on decreases in global mid-ocean ridge axial hydrothermal activity since the Cretaceous, could therefore explain the observed increase in seawater Mg/Ca and Sr/Ca ratios since the Oligocene.

References and Notes

1. J. W. Morse, Q. W. Wang, M. Y. Tsio, *Geology* **25**, 85 (1997).
2. A. L. Cohen, K. E. Owens, G. D. Layne, N. Shimizu, *Science* **296**, 331 (2002).
3. C. H. Lear, H. Elderfield, P. A. Wilson, *Science* **287**, 269 (2000).
4. C. H. Lear, H. Elderfield, P. A. Wilson, *Earth Planet. Sci. Lett.* **208**, 69 (2003).
5. R. A. Berner, A. C. Lasaga, R. M. Garrels, *Am. J. Sci.* **283**, 641 (1983).
6. F. T. Mackenzie, R. M. Garrels, *Am. J. Sci.* **264**, 507 (1966).
7. S. J. Carpenter *et al.*, *Geochim. Cosmochim. Acta* **55**, 1991 (1991).
8. J. A. D. Dickson, *Science* **298**, 1222 (2002).
9. C. H. Lear, Y. Rosenthal, N. Slowey, *Geochim. Cosmochim. Acta* **66**, 3375 (2002).
10. T. Steuber, J. Veizer, *Geology* **30**, 1123 (2002).
11. J. Horita, H. Zimmerman, H. D. Holland, *Geochim. Cosmochim. Acta* **66**, 3733 (2002).
12. T. K. Lowenstein, M. N. Timofeeff, S. T. Brennan, L. A. Hardie, R. V. Demicco, *Science* **294**, 1086 (2001).
13. M. N. Timofeeff, T. K. Lowenstein, M. A. Martins da Silva, N. B. Harris, *Geochim. Cosmochim. Acta* **70**, 1977 (2006).
14. F. M. Richter, D. J. DePaolo, *Earth Planet. Sci. Lett.* **83**, 27 (1987).
15. Materials and methods are available as supporting material on *Science* Online.
16. H. Elderfield, C. G. Wheat, M. J. Mottl, C. Monnin, B. Spiro, *Earth Planet. Sci. Lett.* **172**, 151 (1999).
17. J. C. Alt, D. A. H. Teagle, *Geochim. Cosmochim. Acta* **63**, 1527 (1999).
18. R. M. Coggon, D. A. H. Teagle, M. J. Cooper, D. A. Vanko, *Earth Planet. Sci. Lett.* **219**, 111 (2004).
19. J. M. McArthur, R. J. Howarth, T. R. Bailey, *J. Geol.* **109**, 155 (2001).
20. A. T. Fisher *et al.*, *Nature* **421**, 618 (2003).
21. P. A. Sandberg, *Nature* **305**, 19 (1983).
22. S. M. Stanley, L. A. Hardie, *Palaeogeogr. Palaeoclimatol. Palaeoecol.* **144**, 3 (1998).
23. F. M. Richter, Y. Liang, *Earth Planet. Sci. Lett.* **117**, 553 (1993).
24. T. Steuber, *Int. J. Earth Sci.* **88**, 551 (1999).
25. A. K. Tripati, W. D. Allmon, D. E. Sampson, *Earth Planet. Sci. Lett.* **282**, 122 (2009).
26. D. W. Lea, T. A. Mashiotta, H. J. Spero, *Geochim. Cosmochim. Acta* **63**, 2369 (1999).
27. U. Brand, A. Logan, N. Hiller, J. Richardson, *Chem. Geol.* **198**, 305 (2003).
28. P. S. Freitas, L. J. Clarke, H. Kennedy, C. A. Richardson, F. Abrantes, *Geochim. Cosmochim. Acta* **70**, 5119 (2006).
29. M. T. Gibbs, L. R. Kump, *Paleoceanography* **9**, 529 (1994).
30. K. L. Von Damm, *Geophys. Monogr.* **91**, 222 (1995).
31. R. D. Müller, M. Sdrolias, C. Gaina, B. Steinberger, C. Heine, *Science* **319**, 1357 (2008).
32. M. Seton, C. Gaina, R. D. Müller, C. Heine, *Geology* **37**, 687 (2009).
33. H. J. Paul, K. M. Gillis, R. M. Coggon, D. A. H. Teagle, *Geochem. Geophys. Geosyst.* **7**, Q02003 (2006).
34. J. Gaillardet, B. Dupré, P. Louvat, C. J. Allègre, *Chem. Geol.* **159**, 3 (1999).
35. M. Meybeck, A. Ragu, *River Discharges to the Oceans. An Assessment of Suspended Solids, Major Ions, and Nutrients, Environment Information and Assessment Report* (United Nations Environment Programme, Nairobi, Kenya, 1996).
36. D. Vance, D. A. H. Teagle, G. L. Foster, *Nature* **458**, 493 (2009).

37. This research was supported by National Environment Research Council research grants NER/T/S/2003/00048 and NE/E001971/1 to D.A.H.T. and NE/C513242/1 to R.M.C. and D.A.H.T. This research used samples provided by the Ocean Drilling Program (ODP) and the Integrated Ocean Drilling Program (IODP). ODP was sponsored by NSF and participating countries under the management of Joint Oceanographic Institutions. IODP is supported by NSF; Japan's Ministry of Education, Culture, Sports, Science and Technology; the European Consortium for Ocean Drilling Research; and the People's Republic of China, Ministry of Science and Technology. We thank M. Palmer, P. Wilson, D. Vance, R. James, and three anonymous reviewers for insightful comments that greatly improved this manuscript.

Supporting Online Material

www.sciencemag.org/cgi/content/full/science.1182252/DC1
Materials and Methods
Figs. S1 and S2
Tables S1 to S4
References

21 September 2009; accepted 19 January 2010
Published online 4 February 2010;
10.1126/science.1182252
Include this information when citing this paper.

Climate-Modulated Channel Incision and Rupture History of the San Andreas Fault in the Carrizo Plain

Lisa Grant Ludwig,[1]* Sinan O. Akçiz,[1] Gabriela R. Noriega,[1] Olaf Zielke,[2] J Ramón Arrowsmith[2]

The spatial and temporal distribution of fault slip is a critical parameter in earthquake source models. Previous geomorphic and geologic studies of channel offset along the Carrizo section of the south central San Andreas Fault assumed that channels form more frequently than earthquakes occur and suggested that repeated large-slip earthquakes similar to the 1857 Fort Tejon earthquake illustrate typical fault behavior. We found that offset channels in the Carrizo Plain incised less frequently than they were offset by earthquakes. Channels have been offset by successive earthquakes with variable slip since ~1400. This nonuniform slip history reveals a more complex rupture history than previously assumed for the structurally simplest section of the San Andreas Fault.

Knowledge of the age and associated slip distribution for surface-rupturing earthquakes is essential for understanding fault rupture and the recurrence of large, potentially destructive earthquakes (*1*). Paleoseismological data about previous large earthquakes are needed to characterize rupture patterns and assess the associated seismic hazard (*2*). Dates of past earthquakes are obtained from excavations across active faults, where the disruption of the ground surface at the time of the event is encased in datable sediments. Channels offset along faults are used as markers to determine displacements in successive earthquakes and to infer earthquake recurrence on the basis of two assumptions: (i) Strain release rate along that section of the fault is constant during the period of interest, and (ii) the channels form more frequently than they are offset by earthquakes.

The south central San Andreas Fault (SAF) last ruptured in the great 1857 earthquake (all dates are calendar years C.E.) and displaced channels that crossed the fault (*3*, *4*). In the Carrizo Plain, measurements of slip rate over different time intervals agree with geodetically measured loading rates of ~35 mm/year (*2*, *3*, *5*). Several studies have analyzed offset channels to infer slip distribution from the great 1857 earthquake and prior ruptures (*3*, *4*, *6*–*8*) in the semi-arid Carrizo Plain. Near Wallace Creek (Fig. 1), channels offset by approximately 33 m, 21.8 m, and 9.5 m (*3*, *4*) were interpreted to be caused by three successive earthquakes with surface slip of 11.2 m, 12.3 m, and 9.5 m, respectively (*3*). However, determining the incision age of offset ephemeral stream channels is difficult if only the channel fill sediments are dated, because transported organic material may have inherited age (*7*, *9*–*12*).

We sought to determine the age, and consequently the slip history, of channels that are offset by commonly measured offset values of ~8 to 10 m and ~16 m in the Carrizo Plain and along the 1857 rupture of the southern SAF (*4*, *7*, *8*). To test the hypothesis that incision occurred more frequently than offset, we used traditional stratigraphic analysis, with high-resolution radiocarbon dating and new records of extreme climate events (*9*, *13*, *14*), to determine the relative sequence of earthquake rupture and channel incision. We focused on a section of the SAF between Wallace

[1]Program in Public Health and California Institute for Hazards Research, University of California, Irvine, CA 92697, USA. [2]School of Earth and Space Exploration, Arizona State University, Tempe, AZ 85287, USA.

*To whom correspondence should be addressed. E-mail: lgrant@uci.edu